

# INVESTIGATION OF THE COMBINED EFFECT OF APPENDAGES AND AXIAL POWER PROFILE ON POST-DRYOUT HEAT TRANSFER IN TUBES

H. Zahlan<sup>\*</sup>, D.C. Groeneveld<sup>\*\*†</sup>, L.K.H. Leung<sup>\*\*†</sup>, Aurelian Tanase<sup>\*</sup>, and S.C. Cheng<sup>\*</sup>

<sup>\*</sup>University of Ottawa, Ottawa, ON Canada K1N 6N5

<sup>†</sup>Atomic Energy of Canada Limited, Chalk River, ON Canada K0J 1J0

## Abstract

An experiment has been performed to obtain post-dryout temperature measurements in two vertical Inconel-600 tubes cooled with an upward flow of Refrigerant-134a. One of these tubes exhibited a uniform axial power profile, while the other had a non-uniform axial power profile. The tube with a non-uniform axial power profile was tested in two vertical positions providing measurements in two different profiles. Experiments were carried out in plain and appendage-equipped tubes. The objective of this study is to examine the combined effect of appendages and axial power profile on post-dryout heat transfer. The result shows a strong impact of flow obstacle (shape, size, and pitch) on post-dryout temperature. The effect of axial power profile is noticeable at the developing post-dryout region (attributed mainly to the variation in CHF occurrence), but appears diminishing at the fully developed post-dryout region.

## 1. Introduction

Post-dryout heat transfer is encountered at conditions where critical heat flux (CHF) or CHF temperature has been exceeded. It refers to the heat transfer mode where the vapor phase is in contact with the heated surface and is characterized by the deteriorated heat transfer rate between the heated surface and vapor film. Post-dryout conditions may be encountered in many applications (e.g., steam generators, nuclear reactors, metallurgical processing and cryogenic systems).

Nuclear fuel bundles are equipped with spacing devices designed to maintain the gap size between fuel rods and to reduce vibration by enhanced mechanical rigidity. In general, the axial power profile over these fuel bundles in a power reactor is not uniform; it varies axially and circumferentially, depending mainly on fuelling scheme, fuel burn up and reactivity mechanisms position. A number of studies were performed focusing separately on either the effect of axial power profile (e.g., Becker et al. (1992)) or the effect of appendages (e.g., Leung et al. (2005)) in post-dryout heat transfer. None of these studies have examined the combination of these two effects. The objective of this study is to examine the combined effect of obstacles and axial power profile on post-dryout heat transfer in tubes.

## 2. Experiments

The experiments have been conducted in the multi-fluid test loop at University of Ottawa (Figure 1) using Refrigerant-134a as the working fluid. Test conditions covered a pressure range from

1665 to 2389 kPa (water-equivalent value: 10 to 14 MPa), a mass-flux range from 1395 to 3575  $\text{kg}\cdot\text{m}^{-2}\cdot\text{s}^{-1}$  (water-equivalent value: 2000 to 5000  $\text{kg}\cdot\text{m}^{-2}\cdot\text{s}^{-1}$ ) and an inlet-fluid temperature range from 30 to 70°C (water-equivalent value: 229 to 324°C).

Two test sections (TS's) were used in this investigation: (i) uniform AFD tube, and (ii) inlet/outlet peak AFD tube. These test sections were made of Inconel-600 tubes with an inside diameter of 5.46 mm. Each test section was oriented vertically, heated with direct current (DC) electric power, and cooled with an upward flow. The wall temperature of the test section was measured using K-type self-adhesive thermocouples attached to the outer surface at various locations along the heated length. The non-uniform axial power profile was established by altering the wall thickness (hence electrical resistance) at various locations along the test section. The outer surface was machined down to provide the appropriate wall thickness. This maintains the dimension and smoothness of the inner surface, where the coolant contacted. Figure 2 illustrates the axial power profiles (when tested in both directions) of the non-uniform tube. Yang (2003) provided the detailed description.

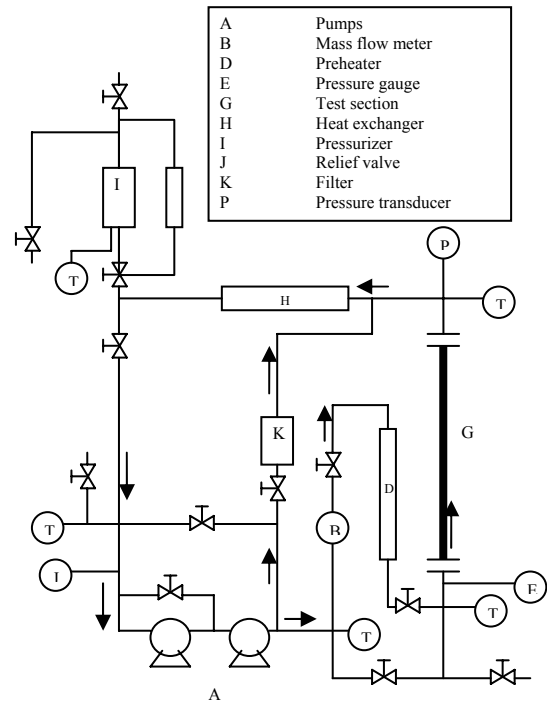


Figure 1 Experimental loop

Mild-steel cylindrical-shaped obstacles of 12% and 24% blockage-area ratios (cross-sectional area of obstacle to the flow area) were introduced inside the test section.

The uniform test section was equipped with four obstacles at 300-mm pitch or seven obstacles at 150-mm pitch. Each obstacle has either blunt or rounded (i.e., streamlined) leading and trailing edges. Each cylindrical obstacle was 10-mm long with a diameter of either 2.74 mm or 1.91mm, which obstructs either 24% or 12%, respectively, of the total flow area. Test sections of inlet-peak and outlet-peak axial power profiles were equipped with either five or nine obstacles. These additional obstacles extended the fully developed PDO region at downstream locations (power increase was limited by CHF occurrence at locations upstream of the first obstacle). Each obstacle was held at the location with a ring-shaped ceramic magnet.

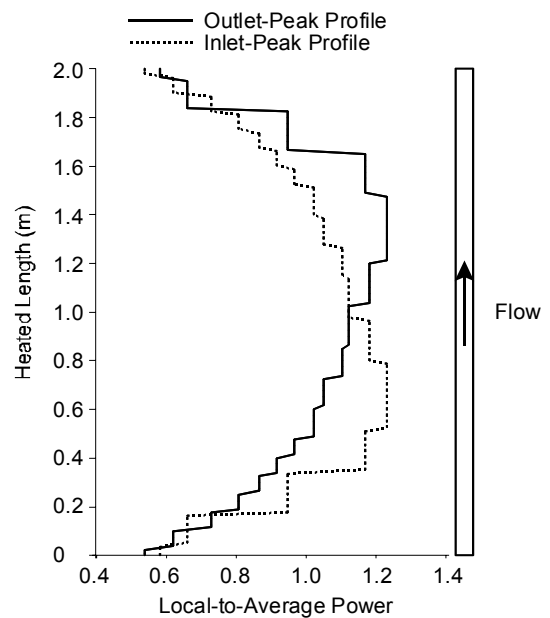


Figure 2 Non-uniform axial power profiles

Post-dryout temperature distributions were recorded at typically five to six power levels at a given set of flow conditions. Measurements were obtained first at the maximum power level corresponding to a maximum surface temperature of 240°C (to avoid Freon decomposition). A scan of flow conditions and surface temperatures was taken. The power was then reduced in steps of 0.15 or 0.3 kW. After reaching steady-state conditions, another scan was recorded at each step until the tube was completely rewetted.

### 3. Results and discussion

Local quality,  $x$ , was calculated from the heat balance and local heat flux,  $q$ , was established from the applied power, heated area, and the power distribution. The local heat-transfer coefficient,  $h$ , was calculated from the local heat flux and experimental wall superheat (i.e.,  $h=q/(T_w-T_b)$ , where  $T_w$  is the calculated inside wall temperature, established from the measured outside wall temperature ( $T_o$ ) using the conduction heat-transfer model, and  $T_b$  is the bulk-fluid temperature).

Relative uncertainties of inside wall temperature ( $U_{T_w}/T_w$ ) and heat transfer coefficient ( $U_h/h$ ) were estimated using the method described in Tavoularis (2005), where 
$$\frac{U_{T_w}}{T_w} = \sqrt{\left(\frac{\partial T_w}{\partial T_o} \frac{T_o}{T_w}\right)^2 \left(\frac{U_{T_o}}{T_o}\right)^2 + \left(\frac{\partial T_w}{\partial q_v} \frac{q_v}{T_w}\right)^2 \left(\frac{U_{q_v}}{q_v}\right)^2 + \left(\frac{\partial T_w}{\partial r_o} \frac{r_o}{T_w}\right)^2 \left(\frac{U_{r_o}}{r_o}\right)^2 + \left(\frac{\partial T_w}{\partial r_i} \frac{r_i}{T_w}\right)^2 \left(\frac{U_{r_i}}{r_i}\right)^2} = 0.02,$$
 similarly for heat transfer coefficient,  $U_h/h = 0.023$ . In this investigation, Q/A repeatability tests were performed for uniform, inlet peak and outlet peak test sections; reasonable agreement between the original experimental data and the repeat points was observed (Figure 3).

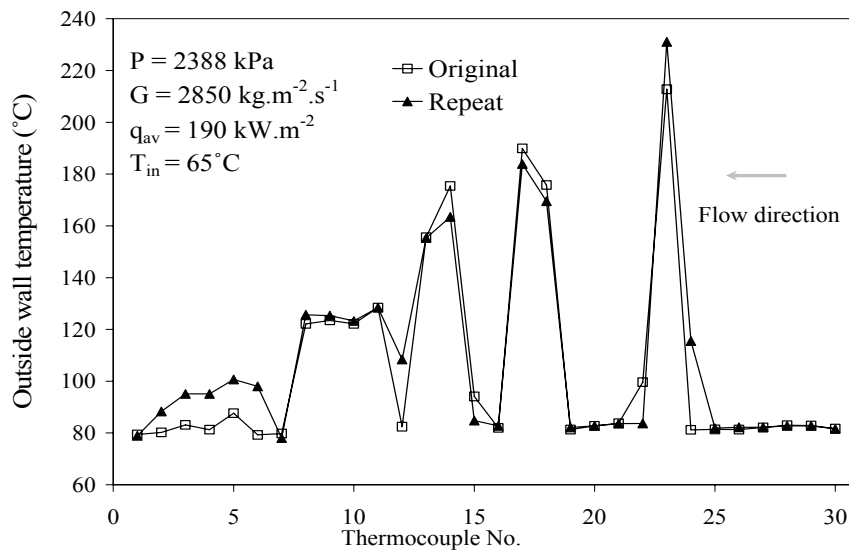


Figure 3 Repeatability test, outlet peak test section (high-pressure and high-mass flux).

Calculated inside-wall temperatures ( $T_w$ ) are compared at various axial locations along test sections of different obstacle configurations. In addition, variations of the inverse heat-transfer coefficient (i.e.,  $h^{-1}$ ) are also shown against local quality for some cases. This facilitates the

assessment of effects of obstacle and axial power profile on post-dryout heat-transfer characteristics at similar local flow conditions.

The following notation system is used to identify the axial power profile and obstacle configuration:  $AbbCddd$  where  $A$  corresponds to either “U”, “IP” or “OP” denoting the uniform, inlet peak, or outlet-peak axial power profile,  $bb$  corresponds to either “12” or “24” denoting the 12% or 24% blockage-area ratio,  $C$  corresponds to “B” or “R” denoting the blunt or round (streamlined) obstacle, and  $ddd$  corresponds to either “150” or “300” denoting either 150-mm or 300-mm obstacle pitch. For example: U24B300 refers to the uniformly heated test section equipped with blunt obstacles having a 24% flow-blockage ratio at the 300-mm pitch.

### 3.1 Pitch effect

Figure 4 illustrates the effect of obstacle pitch on wall-temperature distributions in the uniform-heated tube, which was equipped with either four rounded obstacles at the 300-mm pitch (obstacle numbers 1, 3, 5 and 7) or seven rounded obstacles at the 150-mm pitch (obstacle numbers from 1 to 7). All obstacles had a 24% blockage-area ratio. The reference temperature distribution for a plain (bare) tube is also shown in Figure 4 for comparison. Dryout occurs at the same locations upstream of all obstacles for both pitches. The location differs slightly from that in the plain tube and is probably due to slight differences in flow conditions.

A comparison of wall-temperature distributions of tubes with 150-mm and 300-mm obstacle pitches against those of the bare tube show that the obstacles have a strong effect on delaying dryout occurrence and lowering the post-dryout wall temperature. The developing-flow region extends up to the axial location of about 1 m (red line), and fully developed post-dryout conditions have been reached at locations beyond 1 m in the plain tube (black line). The developing film boiling is caused by the disturbance of droplets impinging on the heated surface and the development of vapour superheat, Guo and Leung (2005). Developing film boiling corresponds to cases downstream of the dryout and transition boiling points where rewetting no longer occurs but the heat transfer is affected by upstream conditions (dryout and/or spacer) and the axial surface temperature distribution has not yet leveled off, Groeneveld and Stewart (1982). The fully developed film boiling region occurs where the axial temperature gradient has reached a plateau and is no longer affected by the distance from the CHF location or spacer location.

Rewetting has been observed at locations just downstream of the obstacle for the 300-mm pitch (only four obstacles were installed for this case and hence the comparison should be focused on every 2<sup>nd</sup> obstacle location shown in Figure 4). Dryout was re-established at locations further downstream of the upstream obstacle until the next obstacle at the downstream location, where rewetting re-occurred. The length of the post-dryout region appears to be longer at the downstream obstacle location than the upstream obstacle location. This is probably due to the reduction in CHF and post-dryout heat-transfer enhancement effects at high qualities. Dryout has been suppressed beyond the first upstream obstacle for the 150-mm pitch, and reestablished at locations slightly upstream of the last obstacle. This results in lower wall temperatures than the obstacle-equipped tube of 300-mm pitch and the plain tube. A drop in wall temperature has

been observed at the last thermocouple location of the obstacle-equipped tubes and is due to the axial heat conduction since the thermocouples are close to the upper power clamp.

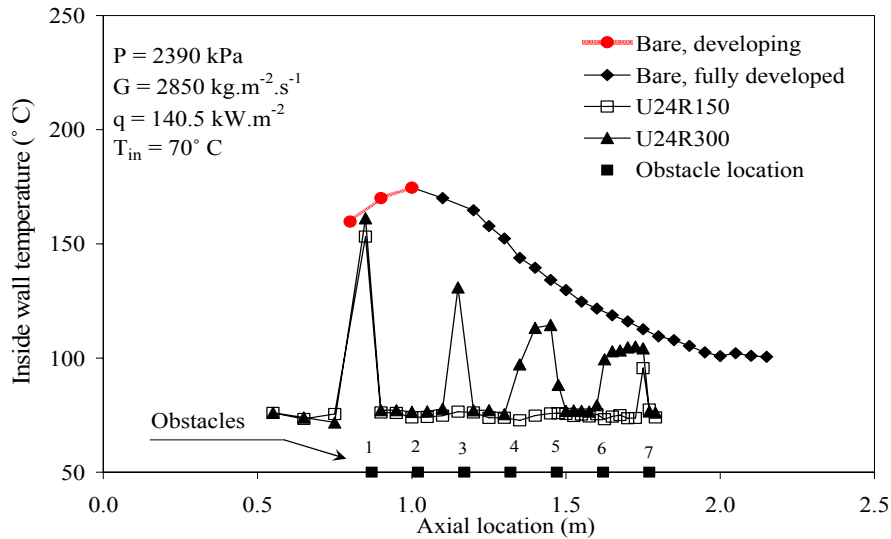


Figure 4 Temperature distributions in uniform-heated tubes with rounded obstacles at different pitches

Figure 5 shows the pitch effect on wall-temperature distributions for blunt-shaped obstacles in the tube with an inlet-peak profile. The distribution for the plain (bare) tube is also shown for comparison. A reduction in wall temperature has been observed for the obstacle-equipped tubes as compared to the plain tube. Dryout occurrences were suppressed by the first upstream obstacle at the 300-mm pitch for locations prior to 0.95 m (only five obstacles were installed in this case and temperature drop corresponded to every 2<sup>nd</sup> obstacle location in Figure 5), and two upstream obstacles at the 150-mm pitch for locations prior to 1.05 m.

The surface appears to rewet at each obstacle location of the 150-mm pitch. Rewetting was observed only at the first three locations (i.e., every 2<sup>nd</sup> of five locations shown in Figure 5) of the 300-mm pitch, while post-dryout conditions appear to be maintained at locations downstream of the last two obstacles. The decreasing trend of wall temperature with increasing axial location signifies reaching of fully developed post-dryout conditions at two downstream sections between obstacles of the 300-mm pitch. Fully developed post-dryout temperature was not established at locations between obstacles of the 150-mm pitch. However, the difference in peak wall temperature between obstacle pitches diminishes at these locations. A peculiar surface-temperature reduction is observed at the second node upstream of the last obstacle; the reduction is probably due to measurement uncertainty of the thermocouples or obstacle location.

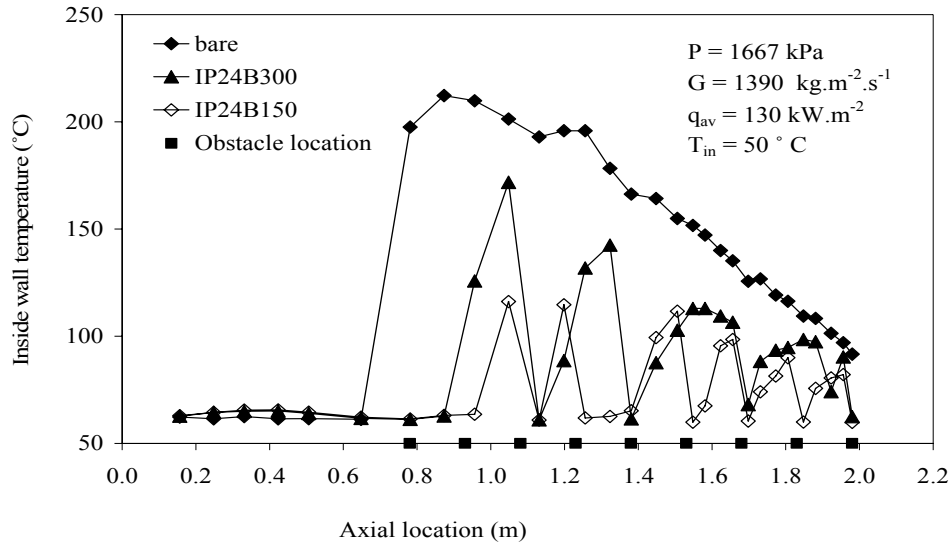


Figure 5 Temperature distributions in tubes of inlet-peak power profile with blunt-shaped obstacles at different pitches

### 3.2 Obstacle-Size effect

Figure 6 compares wall temperatures in tubes equipped with streamlined obstacles of two different sizes (blockage-area ratios of 24% and 12%) at the 300-mm pitch. A large obstacle (24%) suppresses the dryout occurrence over a longer distance than a small obstacle (12%). This is due to the increase in turbulence decay distance downstream of a large obstacle. The difference becomes small with increasing axial location and dryout occurs at the same location beyond 1.5 m. This trend signifies possibly a quality effect on the enhancement due to obstacle size.

Figure 7 compares wall temperatures along tubes having the inlet-peak axial power profile equipped with streamlined obstacles of 24% and 12% blockage-area ratios at a pitch of 300 mm. Peak temperatures of the tube equipped with obstacles of the 12% blockage-area ratio approach those of the bare tube, while peak temperatures of the tube equipped with obstacles of the 24% blockage-area ratio remain lower. The surface rewets at locations of large obstacles, but not of small obstacles. The reduction in wall temperature for the obstacle with a 12% blockage-area ratio appears steeper than anticipated at the location of 1.4 m.

Similar effect of obstacle size on post-dryout wall temperature has been observed in tubes having an outlet-peak axial power profile (Figure 8). Wall temperatures for obstacles of both 24% and 12% blockage-area ratios are lower than those of the bare tube, but the difference between the 24% and 12% PDO temperatures is not significant. Large obstacles tend to suppress dryout re-occurrences over a longer distance downstream of the obstacle than small obstacles. Wall temperatures for the 12% obstacle appear converging to those for the bare tube. Dryout has not occurred for the 24% obstacle over the same location.

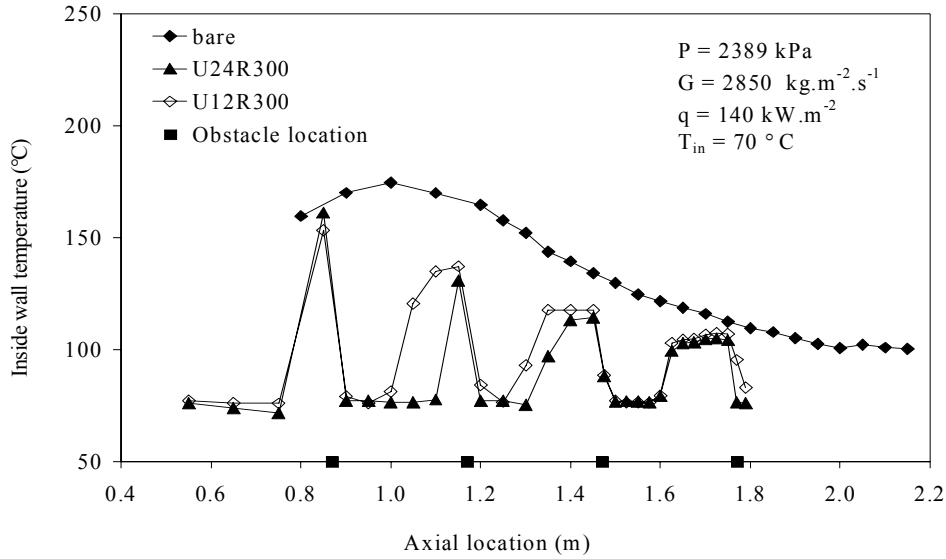


Figure 6 Temperature distributions in tubes of uniform power profile with streamlined obstacles of different sizes

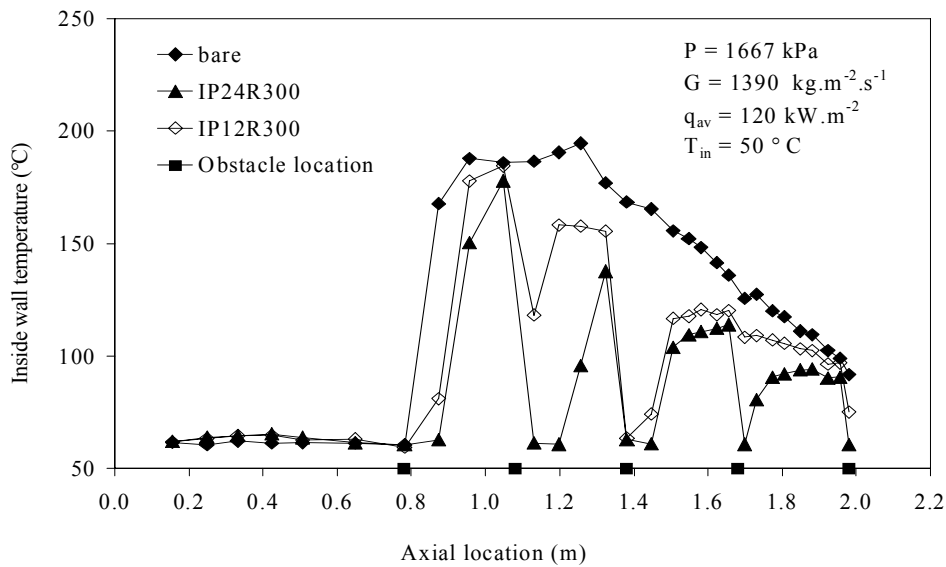


Figure 7 Temperature distributions in tubes of inlet-peak power profile with streamlined obstacles of different sizes

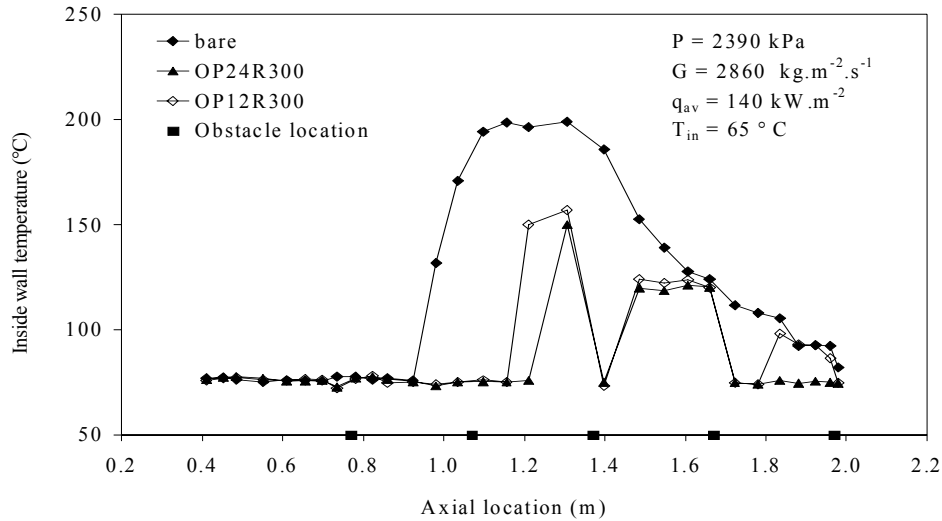


Figure 8 Temperature distributions in tubes of outlet-peak power profile with streamlined obstacles of different sizes

### 3.3 Obstacle-Shape effect

All obstacles used in this experiment had the same cylindrical shape, but the leading and trailing edges of some obstacles were rounded to provide a more streamlined shape than blunt obstacles. Figure 9 compares wall temperatures obtained for these two types of obstacle. Overall, temperature variations are similar for blunt and rounded obstacles. The blunt obstacle, however, appears to suppress dryout re-occurrence over a longer distance than the rounded obstacle. The difference is attributed to the higher turbulence generated from a blunt object than a streamlined object.

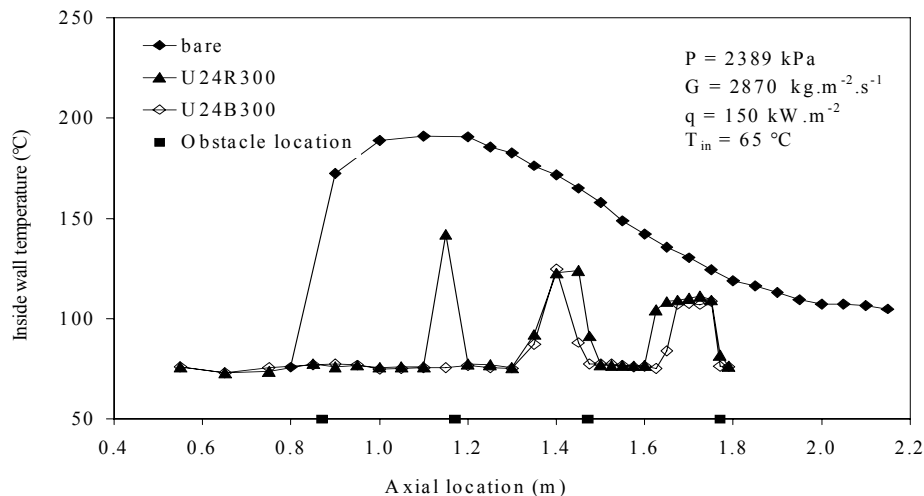


Figure 9 Temperature distributions in tubes of uniform power profile with obstacles of different leading and trailing edges

### 3.4 Axial-Power-Profile effect

Figure 10 shows the impact of axial power profile on post-dryout wall temperatures for streamlined obstacles of 12% blockage-area ratio at the 300-mm pitch. The obstacles are positioned at different locations and the local heat flux varies in tubes of various axial power profiles. Therefore, the comparison of wall temperatures at various locations may not be representative. Overall, wall temperatures of the inlet-peak profile are higher than those of other profiles at upstream locations, while wall temperatures of the uniform profile become high at downstream locations. These differences are attributed mainly to local heat-flux variations between these profiles.

Wall temperatures for obstacle-equipped tubes do not appear varying considerably for these profiles. This is mainly due to the suppression of dryout in the presence of obstacle minimizing the difference in vapour superheat. In general, wall temperatures for the outlet-peak profile are higher than those for other profiles due to the increase in local heat flux.

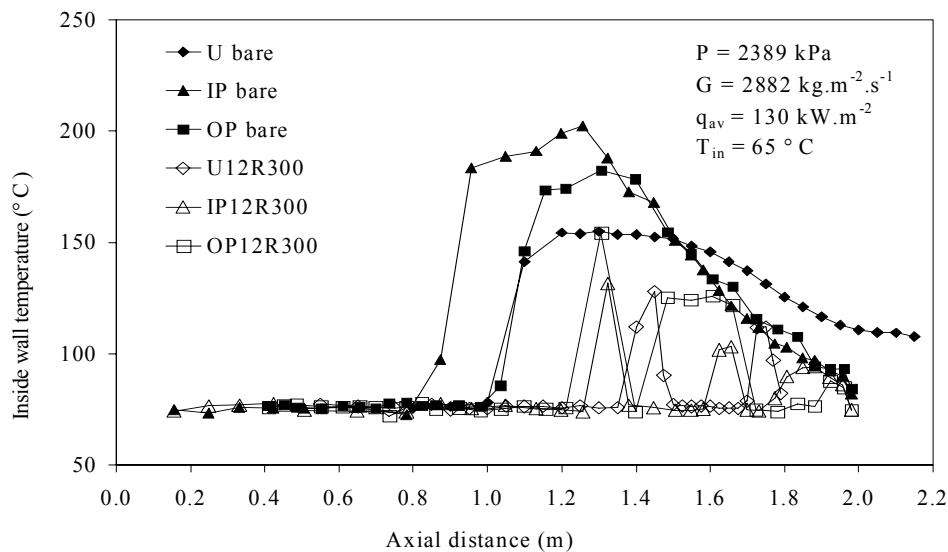


Figure 10 Temperature distributions in tubes of various power profiles with rounded obstacles

As indicated above, comparison of wall temperatures at various locations is difficult due to different obstacle locations in these tubes. In turn, the inverse of heat-transfer coefficient (see Section 3 for description) is presented for tubes of various axial power profiles with respect to local thermodynamic quality. This takes into the account of local conditions variation in the comparison. Figure 11 illustrates variations of inversed heat-transfer coefficient for tubes of various power profiles with rounded obstacles. Differences in inversed heat-transfer coefficient appear to have reduced between tubes of various axial power profiles

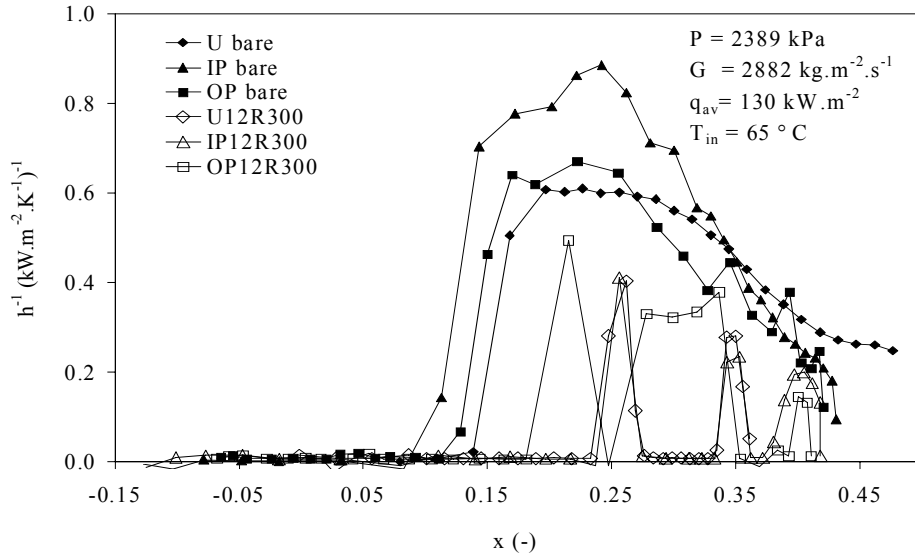


Figure 11 Inversed heat-transfer-coefficients for tubes of various power profiles with rounded obstacles

Overall, the inversed heat-transfer coefficients are larger for the inlet-peak profile at low qualities (beyond dryout), but for the uniform profile at high qualities, than other profiles for bare tubes. Rewetting has been observed at similar local thermodynamic qualities, corresponding to obstacle locations, in tubes of inlet-peak and uniform profile. However, post-dryout conditions, where the inversed heat-transfer coefficient remains large, appear to have maintained at the high local heat-flux section (thermodynamic qualities between 0.25 and 0.35) in tubes of outlet-peak profile.

#### 4. Conclusions

- A unique experimental study has been performed to examine the impact of obstacle and axial power profile on post-dryout heat transfer in tubes. The experiment covered a sufficiently wide range of flow conditions, and provided a vast amount of information and experimental data.
- Flow obstacles significantly decrease the post-dryout wall temperatures and delay the dryout occurrence to downstream locations at similar flow conditions and power. Their impact depends strongly on pitch and size, but weakly on the shape of leading and trailing edges.
- The impact of axial power profile on post-dryout temperature is strong for bare tubes, but diminishes somewhat for obstacle-equipped tubes. The difference is attributed to the dryout suppression and post-dryout heat-transfer enhancement reducing the vapour superheat in the presence of obstacle.

## Acknowledgements

The authors would like to thank Dr. M. El-Nakla for providing the fully developed film-boiling data; financial support is appreciated from Atomic Energy of Canada Limited (AECL) and the Natural Sciences and Engineering Research Council (NSERC) of Canada.

## 5. References

Becker, K.M., Askeljung, P., Hedberg, S., Söderquist, B. and Kahlbom, U., “An Experimental Investigation of the Influence of Axial Heat Flux Distributions on Post Dryout Heat Transfer for Flow of Water in Vertical Tubes”, KTH-NEL-54, 1992

Groeneveld, D. C. and Stewart, J. C., “The Minimum Film Boiling Temperature for Water during Film Boiling Collapse”, Proc. 7<sup>th</sup> International Heat Transfer Conference, Munich, Vol. 4, pp. 303-308, 1982

Leung, L.K.H., Groeneveld, D.C. and Zhang, J., “Prediction of the Obstacle Effect on Film-Boiling Heat Transfer”, *Nuclear Engineering and Design*, 235 (6), pp. 687 – 700, 2005

Guo, Y., Leung, L.K.H., “Developing Film Boiling Heat Transfer in Tubes, NURETH-11 Avignon, France, October 2005

Yang, J., “Effect of non-uniform axial heat-flux distribution on critical heat flux”, M.A.Sc. thesis, University of Ottawa, Ottawa, Canada, December 2003

Tavoularis, S., “Measurement in Fluid Mechanics”, Cambridge University Press, 2005

## Nomenclature

G	mass flux	(kg m <sup>-2</sup> s <sup>-1</sup> )
h	heat transfer coefficient	(kW m <sup>-2</sup> K <sup>-1</sup> )
p	pressure	(kPa)
q	heat flux	(kW m <sup>-2</sup> )
q <sub>v</sub>	volumetric density of heat source	(kW m <sup>-3</sup> )
T	temperature in degrees Celsius	(°C)
x	thermodynamic quality = (H - H <sub>f</sub> ) / H <sub>fg</sub>	(-)
z	axial location	(m)
r	tube radius	(m)
Q/A	quality assurance	

## Subscripts

av	average
i	inside
o	outside
w	wall